THE JOURNAL OF PHYSICAL CHEMISTRY C
A JOURNAL OF THE AMERICAN CHEMICAL SOCIETY

pubs.acs.org/JPCC

Article

# Tuning Molecular Emission: Exploring Plasmonic Coupling Effects across High and Low Quantum Yields

*Published as part of The Journal of Physical Chemistry C special issue "Naomi Halas and Peter Nordlander Festschrift".*

Stavros Athanasiou* and Olivier J. F. Martin*

Cite This: *J. Phys. Chem. C* 2025, 129, 4282−4289

Read Online

ACCESS | Metrics & More | Article Recommendations | Supporting Information

**ABSTRACT:** The interaction between molecules and plasmonic nanoparticles significantly influences molecular emission properties, offering opportunities to enhance fluorescence through the Purcell effect and strong coupling phenomena. While previous studies have focused on high quantum yield molecules, the role of molecular spectral tuning across varying quantum yield regimes remains underexplored. In this work, we investigate the fluorescence enhancement of molecules coupled to pNPs, analyzing how intrinsic quantum yield, molecular absorption and emission wavelengths, and plasmonic particle properties interact to optimize fluorescence. We establish a clear connection between the particle's scattering characteristics and the conditions for optimal enhancement, showing that for moderate quantum yields, maximal fluorescence can occur off-resonance. In contrast, for low quantum yields, particle absorption is minimized, and enhancement peaks at plasmon resonance. These insights, supported by examples, provide valuable guidance for designing systems in the near- and mid-infrared, where quantum yield limitations are pronounced due to the energy-gap law. Our findings pave the way for advancements in applications such as fluorescence imaging, light-fidelity communications, and optical security.

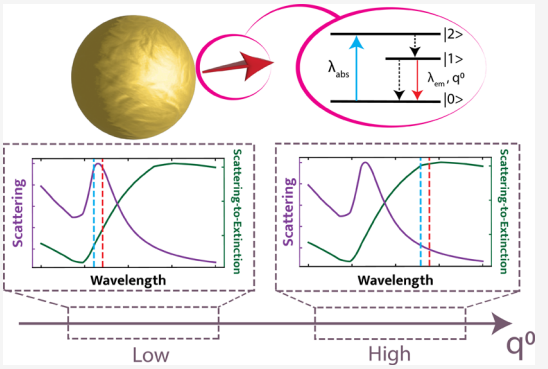


## INTRODUCTION

The interaction between a molecule and a plasmon mode has profound effects on the molecule's emission properties. One of the most significant outcomes of this interaction is the modification of the spontaneous emission rate through the Purcell effect,[1] which enhances the emission rate by tailoring the local density of states under the weak coupling condition.[2] When the interaction becomes strong, additional intriguing phenomena appear,[3] including the formation of hybrid light-matter states, which can dramatically alter the molecule's emission characteristics.[4]

This type of molecule−plasmon interaction is achievable near metal-dielectric interfaces[5] and in the presence of plasmonic nanoparticles (pNPs).[6−8] Although plasmonic cavities are typically associated with a low quality factor, their high spatial confinement can nonetheless significantly enhance light-matter interactions.[9] Numerous factors influence this effect, including the geometry and material of the plasmonic particle, as well as the position of the emitter and the dipole orientation.[7,8,10−14] These parameters govern the pNP-emitter coupling, and thereby the resulting fluorescence enhancement.

One of the key parameters is the intrinsic quantum yield $q^0$, which dictates the magnitude of enhancement in this coupled system. Specifically, the enhancement is inversely proportional to $q^0$. In real molecules, the intrinsic quantum yield tends to follow a specific trend: in the visible part of the electromagnetic spectrum, organic dyes exhibit near-unity yields.[15,16] However, due to the energy gap law, the yield decreases dramatically in the near-infrared region.[15,17,18] Hence, there is a significant need to enhance the light emission of these dyes for applications in the near-infrared and mid-infrared domains such as light-fidelity communications,[19,20] fluorescence imaging[21,22] and optical security.[23] Coupling these dyes with plasmonic particles can substantially improve light emission by leveraging field confinement and amplification. It should be noted that a similar trend in the intrinsic quantum yield is also

**Received:** December 20, 2024
**Revised:** February 7, 2025
**Accepted:** February 10, 2025
**Published:** February 14, 2025

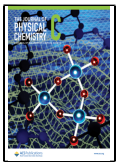





https://doi.org/10.1021/acs.jpcc.4c08617
*J. Phys. Chem. C* 2025, 129, 4282−4289

observed in quantum dots, particularly in the mid-infrared regime, although driven by different mechanisms.[16]

Although the pNP−molecule system has been studied for nearly two decades, much of the focus has been on molecules with high quantum yields and fixed molecular spectral configurations with respect to the pNP. To the best of our knowledge, a comprehensive study on spectral tuning across both high- and low-quantum-yield regimes is still lacking. In this work, we provide such a description for arbitrary quantum yields, by analyzing the enhancement factors with respect to key molecular properties, namely the absorption and emission wavelengths, and the intrinsic quantum yield, while fixing the inhomogeneous electromagnetic environment defined by the pNP. Through this approach, we elucidate the connection between a molecule's spectral configuration and its intrinsic quantum yield, and present examples to illustrate and support these findings.

Our study is structured as follows: Section Methods provides a concise overview of the theoretical background, highlighting the key quantities relevant to this work. In Results and Discussion, we present and discuss our results. We demonstrate the connection between the modified molecular rates and the particle response, and use this relationship to show that the spectral tuning of the molecule for optimal enhancement depends on the quantum yield. Several examples are provided, offering insights into the results and addressing practical considerations. Finally, in Conclusions, we summarize our key findings.

## METHODS

We now briefly introduce the setup of our system and the quantities of interest.[24] Consider a spherical pNP in vacuum such as the one in Figure 1, situated at the origin of our coordinate system. A molecule with an absorption wavelength $\lambda_{abs}$, emission wavelength $\lambda_{em}$ and intrinsic quantum yield $q^0$ is placed in the vicinity of this particle at a location $\mathbf{r} = r\hat{\mathbf{x}}$, and the combined system is illuminated by a monochromatic plane wave with wavelength $\lambda$ propagating along the $z$-direction and polarized along the $x$-direction. The molecule's dipole moment $\mathbf{p} = p\hat{\mathbf{x}}$ is oriented perpendicular to the surface of the particle.

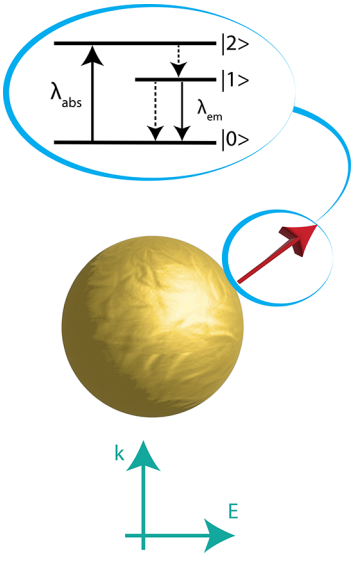


**Figure 1.** Illustration of the pNP-molecule system illuminated by a plane wave with wavenumber $k$ and electric field component $E$, with the molecule depicted as a 3-level system, showing its absorption/excitation wavelength $\lambda_{abs}$ and the emission wavelength $\lambda_{em}$.

The fluorescence signal in the steady state, generated by an ensemble of $N$ noninteracting molecules, is given by the following simple expression[2,7] (for details, see Section S1 in the Supporting Information)

$$S = \gamma_{fl} N \tag{1}$$

where $N$ is the total number of molecules (or concentration of molecules). The fluorescence rate $\gamma_{fl} = \gamma_{exc}\, q$ is defined as the product of the excitation rate $\gamma_{exc}$ and the quantum yield $q$. In the presence of the pNP, the fluorescence rate is modified with respect to that of free space

$$\begin{aligned} F_{fl}(\mathbf{r},\ \lambda_{abs},\ \lambda_{em},\ q^0) &= \frac{S}{S_0} \\ &= \frac{\gamma_{exc}(\mathbf{r},\ \lambda_{abs})}{\gamma^0_{exc}(\lambda_{abs})} \frac{q(\mathbf{r},\ \lambda_{em},\ q^0)}{q^0} \\ &= F_{exc}(\mathbf{r},\ \lambda_{abs}) F_{em}(\mathbf{r},\ \lambda_{em},\ q^0) \end{aligned} \tag{2}$$

where $F_{exc}$ is the excitation enhancement factor, $F_{em}$ is the emission modification factor and $q^0$ is the intrinsic quantum yield.

The factor $F_{exc}$ quantifies the modification of the excitation rate due to the presence of the pNP and is defined as the following ratio:

$$F_{exc}(\mathbf{r},\ \lambda_{abs}) = \frac{|\hat{\mathbf{p}}\cdot\mathbf{E}_{tot}(\mathbf{r},\ \lambda_{abs})|^2}{|\hat{\mathbf{p}}\cdot\mathbf{E}_{inc}|^2} \tag{3}$$

where $\hat{\mathbf{p}}$ is the direction of the dipole moment. $F_{exc}$ is computed using the total field $\mathbf{E}_{tot} = \mathbf{E}_{inc} + \mathbf{E}_{sca}$ at $\mathbf{r}$, where $\mathbf{E}_{sca}$ is the scattered field from a spherical particle under plane wave illumination, provided by the Mie theory,[25,26] and $\mathbf{E}_{inc}$ is the incident field. The resulting excitation enhancement factor reads

$$F_{exc}(\mathbf{r},\ \lambda_{abs}) = \left| \sum_{n=1}^{\infty} i^{n+1}(2n+1) P_n^1(0) \left[ \frac{j_n(kr) - a_n(\omega) h_n^{(1)}(kr)}{kr} \right] \right|^2 \tag{4}$$

where $P_n^1(0)$ is an associated Legendre polynomial, $k = k_0 n_2$ is the wavevector in a background medium $n_2$, $j_n(kr)$ is the spherical Bessel function of the first kind, $h_n^{(1)}(kr)$ the spherical Hankel function of the first kind and $a_n(\omega)$ is the Mie scattering coefficient (see also Section S1 in Supporting Information).

The emission modification factor $F_{em}$ is the ratio of the modified quantum yield $q$ to $q^0$, where $q$ is given by

$$\begin{aligned} q(\mathbf{r},\ \lambda_{em},\ q^0) &= \frac{\gamma_{rad}(\mathbf{r},\ \lambda_{em})}{\gamma_{rad}(\mathbf{r},\ \lambda_{em}) + \gamma_q(\mathbf{r},\ \lambda_{em}) + \gamma^0_{nr}} \\ &= \frac{F_{rad}(\mathbf{r},\ \lambda_{em})}{F_{rad}(\mathbf{r},\ \lambda_{em}) + F_q(\mathbf{r},\ \lambda_{em}) + \frac{1}{q^0} - 1} \end{aligned} \tag{5}$$



https://doi.org/10.1021/acs.jpcc.4c08617
J. Phys. Chem. C 2025, 129, 4282−4289

Radiative losses both due to the plasmon mode and the emitter are described by the radiative enhancement factor

$$F_{\mathrm{rad}}(\mathbf{r},\ \lambda_{\mathrm{em}}) = \frac{\gamma_{\mathrm{rad}}(\mathbf{r},\ \lambda_{\mathrm{em}})}{\gamma_{\mathrm{rad}}^{0}} = \frac{3}{2}\sum_{n} n(n+1)(2n+1)\ \frac{|j_n(kr) - a_n(\omega)h_n^{(1)}(kr)|^2}{(kr)^2} \tag{6}$$

In the presence of the nanoparticle, an additional nonradiative channel arises due to Ohmic losses within the particle, represented by the quenching factor

$$F_q(\mathbf{r},\ \lambda_{\mathrm{em}}) = \frac{\gamma_q(\mathbf{r},\ \lambda_{\mathrm{em}})}{\gamma_{\mathrm{rad}}^{0}} = \frac{3}{2}\sum_{n} n(n+1)(2n+1)\left|\frac{h_n^{(1)}(kr)}{kr}\right|^2 \mathrm{Re}\left\{a_n(\omega) - |a_n(\omega)|^2\right\} \tag{7}$$

We use these analytical expressions to describe the modification of the fluorescence rate in the presence of a spherical pNP.[27−29]

Our upcoming analysis assumes interaction with a single radiating mode, specifically the dipolar mode. In this case, the scattering cross section of the particle provides insights into the near-field enhancement, taking into account the near-field spatial profile as well. If higher-order modes were present, adjustments to the molecular parameters would be necessary to achieve optimal enhancement.

## RESULTS AND DISCUSSION

For the first part of our study, we consider a spherical gold nanoparticle with radius of $R$ = 50 nm. The dielectric function of gold is taken from the literature.[30] A molecule with a given quantum yield $q^0$ and spectral configuration ($\lambda_{\mathrm{abs}}$, $\lambda_{\mathrm{em}}$) is placed near the particle at a distance $h = r - R$. Its fluorescence rate is modified accordingly to this distance, as the molecule is exposed to the inhomogeneous electromagnetic environment set by the plasmonic nanoparticle, as illustrated In Figure 2a; this dependence is well-known in the literature.[7,12,31] There exists a distance $h_{\mathrm{opt}}$ at which fluorescence is optimally enhanced. This radiation enhancement results mainly from the coupling of the emitter to the dipole mode of the nanoparticle and becomes increasingly important as the emitter approaches the particle. However, for very small $h$, fluorescence is quenched due to coupling to the nonradiative modes of the particle (see Figure S2 in the Supporting Information), while for $h \to \infty$, the value of free space is approached. Therefore, fluorescence enhancement involves an interplay between radiative and nonradiative losses in the particle.

Let us now vary independently the two molecular wavelengths $\lambda_{\mathrm{abs}}$ and $\lambda_{\mathrm{em}}$, considering $q^0 = 1$ for the moment. Figure 2b, shows the optimized fluorescence enhancement with respect to $h$,

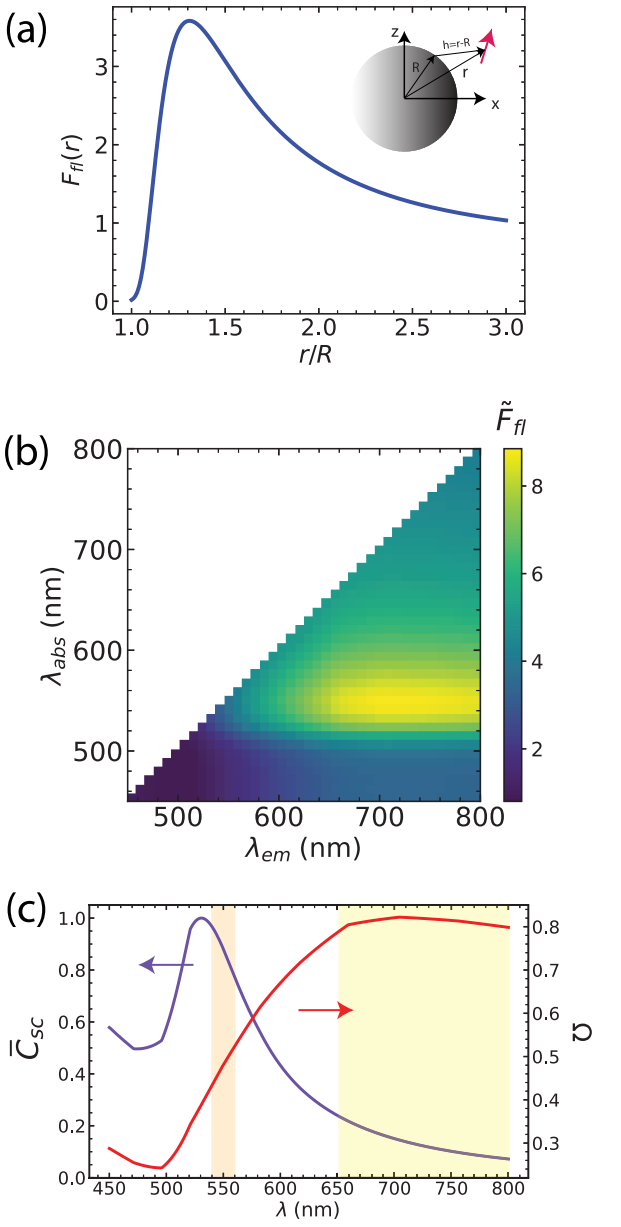


**Figure 2.** Enhancing fluorescence of a molecule with arbitrary $\lambda_{\mathrm{abs}}$, $\lambda_{\mathrm{em}}$ and $q^0$ = 1, with a $R$ = 50 nm gold pNP. (a) Fluorescence modification factor $F_{\mathrm{fl}}$ as a function of the location of the molecule $r$ (in units of $R$). The inset serves as a guide to the different length quantities. This result is obtained for a molecule with $\lambda_{\mathrm{abs}}$ = 530 nm, $\lambda_{\mathrm{em}}$ = 550 nm. (b) Spectrally resolved enhancement factor $\tilde{F}_{\mathrm{fl}}$ as a function of the molecular wavelengths. (c) Normalized scattering cross section $\bar{C}_{\mathrm{sc}}$ and scattering-to-extinction ratio Ω of the gold pNP. The shaded orange (yellow) region corresponds to the values of $\lambda_{\mathrm{abs}}$ ($\lambda_{\mathrm{em}}$) at which $\tilde{F}_{\mathrm{fl}}$ is optimal (within 5% of the numerically computed maximum value).

$$\tilde{F}_{\mathrm{fl}}(\lambda_{\mathrm{abs}},\ \lambda_{\mathrm{em}}) = \max_{h}\{F_{\mathrm{fl}}(h+R,\ \lambda_{\mathrm{abs}},\ \lambda_{\mathrm{em}},\ q^0 = 1)\} \tag{8}$$

as a function of $\lambda_{\mathrm{abs}}$, $\lambda_{\mathrm{em}}$. The bright yellow region indicates the optimal $\tilde{F}_{\mathrm{fl}}$ with respect to the molecular wavelengths, which we will refer to as the optimal spectral region from now on. This region occurs when $\lambda_{\mathrm{abs}}$ values are near the plasmon resonance wavelength in the normalized scattering cross section $\bar{C}_{\mathrm{sc}}$, while $\lambda_{\mathrm{em}}$ falls within the wavelength range


https://doi.org/10.1021/acs.jpcc.4c08617
J. Phys. Chem. C 2025, 129, 4282−4289

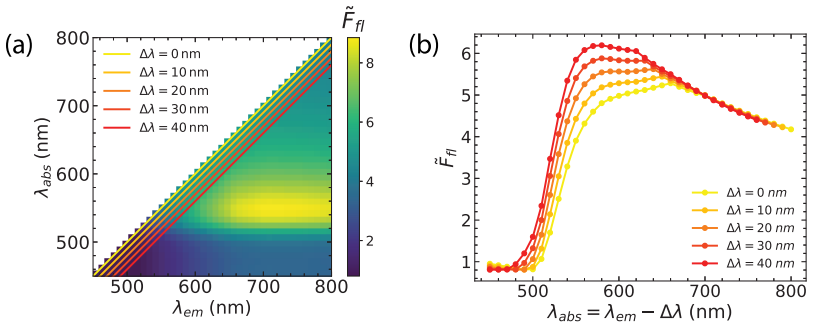


**Figure 3.** Spectrally resolved fluorescence $\tilde{F}_{fl}$ with constraints. (a) Lines of the form $\lambda_{abs} = \lambda_{em} - \Delta\lambda$ are drawn for various values of $\Delta\lambda$. (b) The enhancement factor $\tilde{F}_{fl}$ as a function of the $\lambda_{abs}$ (or equivalently of $\lambda_{em}$), as extracted from (a). Here, we use a gold pNP with $R$ = 50 nm and further $q^0 = 1$ (as in Figure 2).

where the scattering-to-extinction ratio $\Omega$ is maximized, as shown in Figure 2c. The scattering-to-extinction ratio, defined as $\Omega = C_{sca}/C_{ext} = C_{sca}/(C_{sca} + C_{abs})$, measures the particle's efficiency to scatter light relative to extinction. The orange (yellow) band in Figure 2c represents the range of $\lambda_{abs}$ ($\lambda_{em}$) for which $\tilde{F}_{fl}$ is optimal. We define "optimal" as being within 5% of the numerically computed maximum value of $\tilde{F}_{fl}$, a practice that is suitable for practical applications. This analysis reveals a connection between optimal fluorescence enhancement and the nanoparticle's response to plane wave illumination. The excitation rate is modified due to the particle's enhanced near-field, which reaches its peak at the plasmon resonance wavelength. The slight shift between the resonance and the yellow band in Figure 2c is attributed to the near-field shift relative to the far-field response.[32] The emission rate achieves optimal enhancement within the wavelength range where $\Omega$ is highest. In this range, scattering dominates over absorption and creates ideal conditions for enhancing the emission process. Although the emission process is studied with a classical pNP−radiating-dipole system, the theory reveals a connection between this system and the particle's scattering properties (under plane wave illumination) due to the presence of the Mie scattering coefficients in both circumstances (compare eqs 6 and 7 with eqs S14 and S16 from Supporting Information). Ultimately, the particle's response acts as a guide to identifying conditions that achieve optimal enhancement.

This discussion extends beyond gold spherical pNPs as demonstrated with other plasmonic materials such as Silver (Ag) and Zirconium Nitride (ZrN). We provide a similar analysis for these materials in the Supporting Information, specifically in Figures S3 and S4. The case of ZrN is akin to that of gold; however, for silver, we observe that the scattering-to-extinction ratio is already optimized at the plasmon resonance wavelength, resulting in $\tilde{F}_{fl}$ being optimal at this point. The characteristics of the optimal region are significantly influenced by the material properties. This effect can be effectively illustrated using the simple Drude model, as shown in Figure S1 of the Supporting Information. Increasing the intrinsic losses by varying the damping rate $\gamma$ results in a broader optimal region and a reduced magnitude of enhancement.

In the case of real molecules, the two molecular wavelengths differ by a (Stokes) shift $\Delta\lambda$ that can vary from molecule to molecule. We identify this practical situation by taking lines of the form $\lambda_{abs} = \lambda_{em} - \Delta\lambda$, as in Figure 3a, and isolating them in Figure 3b. For small values of $\Delta\lambda$, $\tilde{F}_{fl}$ is optimized away from the plasmon resonance wavelength, and likewise in the case of $\Delta\lambda$ = 40 nm, which corresponds to ($\lambda_{abs}$, $\lambda_{em}$) = (580, 620) nm. For typical organic dyes,[15] the Stokes' shift is around 10−20 nm, and those optical species follow the relevant curves in Figure 3b.

Interesting features arise for an nonunity quantum yield, which are seldom studied in the literature. To solely focus on the impact of yield, we consider the optimal enhancement factor with respect to all $h$, $\lambda_{abs}$, $\lambda_{em}$,

$$\mathcal{F}(q^0) = \max_{\lambda_{abs},\lambda_{em}} \tilde{F}_{fl}(\lambda_{abs}, \lambda_{em}, q^0) \tag{9}$$

The absorption and emission wavelengths where $\mathcal{F}$ is found are denoted by $\Lambda_{abs}$ and $\Lambda_{em}$; they also depend on the yield. For practical purposes, we will relax the condition of optimal enhancement to about 5% of the previously described maximum enhancement value, and thus the wavelengths $\Lambda_{abs}$, $\Lambda_{em}$ will now correspond to a range of wavelengths. The impact of a decreasing quantum yield is apparent in Figure 4a−c for $q^0$ = 0.1, $q^0$ = 0.01 and $q^0$ = 0.001 respectively. One immediate observation is the enhancement magnitude, which increases with decreasing quantum yield. More importantly, the optimal region is blue-shifted along the $\lambda_{em}$ axis, but not along the $\lambda_{abs}$ axis. This is expected, as only the $F_{em}$ factor is influenced by the quantum yield change. Figure 4d shows the overall evolution of $\mathcal{F}$ and $\Lambda_{em}$ as a function of $q^0$. The curve for $\mathcal{F}$ follows the expected $1/q^0$ behavior and the $\Lambda_{em}$ zone appears to shift toward smaller values as $q^0$ decreases. Thus, for very small quantum yields the optimal region is centered near the plasmon resonance wavelength in both $\lambda_{abs}$ and $\lambda_{em}$.

We examine this observation by rewriting the emission enhancement as

$$F_{em} = \frac{F_{rad}}{q^0[F_{rad} + F_q - 1] + 1} \tag{10}$$

Let us first consider the limit of $h \to 0$. In this limit, regardless of the value of $q^0$, the quenching factor is much larger than the radiative enhancement factor $F_q \gg F_{rad} - 1$, thus we may approximate the emission enhancement factor as follows

$$F_{em} \approx \frac{F_{rad}}{q^0 F_q + 1} \tag{11}$$

There seems to be an interplay between the yield and the quenching factor: for moderate yields, we expect $q^0 F_q \gg F_{exc}F_{rad}$ and thus $F_{em} \to 0$ at small distances. However, for very small yields (we avoid the exact case of $q^0 = 0$), we have $q^0 F_q \sim 0$ and thus


https://doi.org/10.1021/acs.jpcc.4c08617
J. Phys. Chem. C 2025, 129, 4282−4289

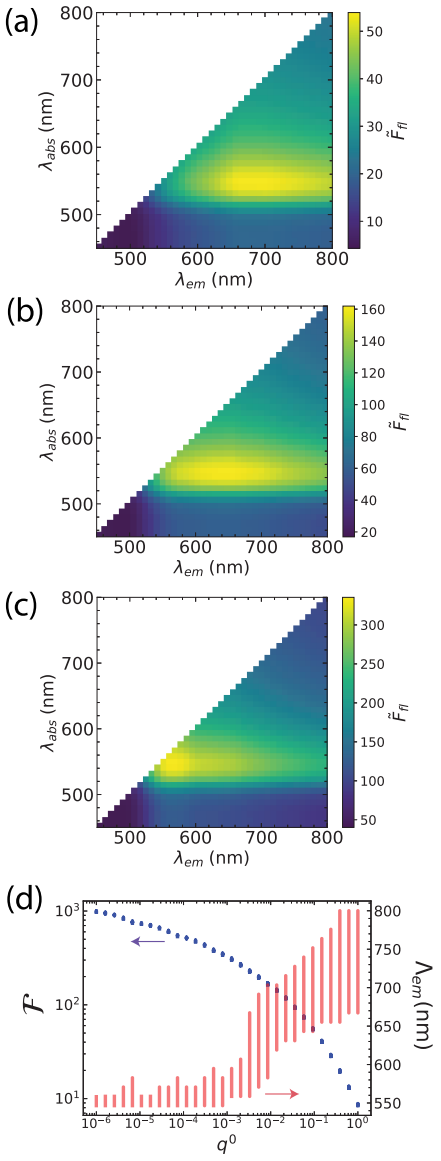


**Figure 4.** Quantum yield dependence of the spectrally resolved fluorescence enhancement for a gold pNP with $R$ = 50 nm. This is illustrated for (a) $q^0$ = 0.1, (b) $q^0$ = 0.01 and (c) $q^0$ = 0.001. In (d), this dependence is summarized for a range of $q^0$ values. The secondary vertical axis (right axis) is the corresponding emission wavelength range $\Lambda_{em}$ (within 5% of the numerically computed maximum value).

$$\lim_{q^0 \to 0} F_{em} = F_{rad} \tag{12}$$

and $F_{fl} \to F_{exc}F_{rad}$. This result holds for any value of $h$ in the limit of $q^0 \to 0$. The quenching factor becomes negligible. Both the excitation and radiative enhancement are expected to be maximal when the spectral configuration of the molecule is aligned with the plasmon resonance peak. Overall, poor emitting dyes crucially benefit from placing them arbitrarily close to the particle, as far as the linear response model is concerned. At very small distances, electron spilling and other effects become important, typically at distances $h \leq 1$ nm.[33−35]

We have extended our analysis to other values of the particle radius $R$. The transition of $\Lambda_{em}$ toward the plasmon resonance wavelength depends on the pNP radius (see Figure S5 in Supporting Information). Small-sized particles are prone to greater Ohmic losses, thus decreasing the overall scattering-to-extinction ratio, and increasing the quenching factor $F_q$. This leads to a slower transition toward the plasmon resonance because the quantum yield needs to overcome the large value of $F_q$. Since $F_q$ increases with decreasing radius, it implies that the transition point will occur at an even smaller quantum yield.

Let us now examine a few examples. We consider two dyes of arbitrary $q^0$, one with an on-resonance configuration of $\lambda_{abs}$ = 520 nm, $\lambda_{em}$ = 540 nm (Dye 1) and one with an off-resonance configuration of $\lambda_{abs}$ = 657 nm, $\lambda_{em}$ = 677 nm (Dye 2). They are shown in Figure 5a, relative to the normalized scattering cross section and scattering-to-extinction ratio of the pNP. For a quantum yield of $q^0$ = 1, Dye 2 exhibits larger enhancement in the fluorescence rate compared to Dye 1. The low $\Omega$ value at the plasmon resonance significantly reduces the emission enhancement and subsequently $F_{fl}$. However, the low scattering efficiency away from the resonance (and in the range of wavelengths where $\Omega$ is large) does not result in the dramatic decrease observed in Dye 1 at the plasmon resonance wavelength (where $\Omega$ is small). Consequently, $F_{fl}$ remains greater for Dye 2. As the quantum yield is decreased, we identify a value of the quantum yield ($q^0$ = 0.01) at which the magnitude of $F_{fl}$ becomes equal for both dyes, as depicted in Figure 5c. The excitation and emission rates are enhanced in such a manner that the product of the respective modification factors yield identical $F_{fl}$. When the quantum yield is further reduced and acquires a very small value (low-quantum-yield regime), Dye 1 exhibits greater enhancement compared to Dye 2. This result is consistent with our previous findings, in which notably particle absorption becomes negligible. Note that in this example, the quantum yield is not low enough to completely suppress particle absorption. However, it is sufficiently small for absorption to be treated as a correction, meaning the dye still experiences some degree of quenching when it is positioned very close to the particle. The reduced influence of particle absorption with decreasing quantum yield can also be justified by examining the optimal dye position $r_{opt}$, which shifts to smaller values, as shown in Figure 5b−d. In the regime of very low quantum yields, the excitation and emission rates are maximally enhanced near the plasmon resonance and thus, the spectral configuration of Dye 1 becomes the desired one.

Another example complements our findings: consider two spherical pNPs made of different materials: gold Au and doped tungsten oxide $WO_{2.83}$,[36] along with a single dye characterized by an arbitrary quantum yield and a spectral configuration of $\lambda_{abs}$ = 880 nm and $\lambda_{em}$ = 900 nm, as shown in Figure 6a,b. This example illustrates a practical scenario: enhancing the light emission of a given dye in the near-infrared−experiencing reduction of the intrinsic quantum yield due to the energy-gap law−using a selection of pNPs of different materials in order to choose the optimal one. The dye is positioned near the plasmon resonance of the $WO_{2.83}$ pNP, while it is quite far from the resonance of the gold pNP. We study the optimal enhancement $\mathcal{F}$ as a function of the quantum yield for both cases. In Figure 6c, we identify two distinct zones, which are highlighted with the color of the material that enhances the most, while also indicating the transition point where one material takes over the other to provide the strongest enhancement. In the Au-optimized zone, the emission enhancement away from the resonance is significant and the same arguments as previously applied. As we decrease the


https://doi.org/10.1021/acs.jpcc.4c08617
J. Phys. Chem. C 2025, 129, 4282−4289

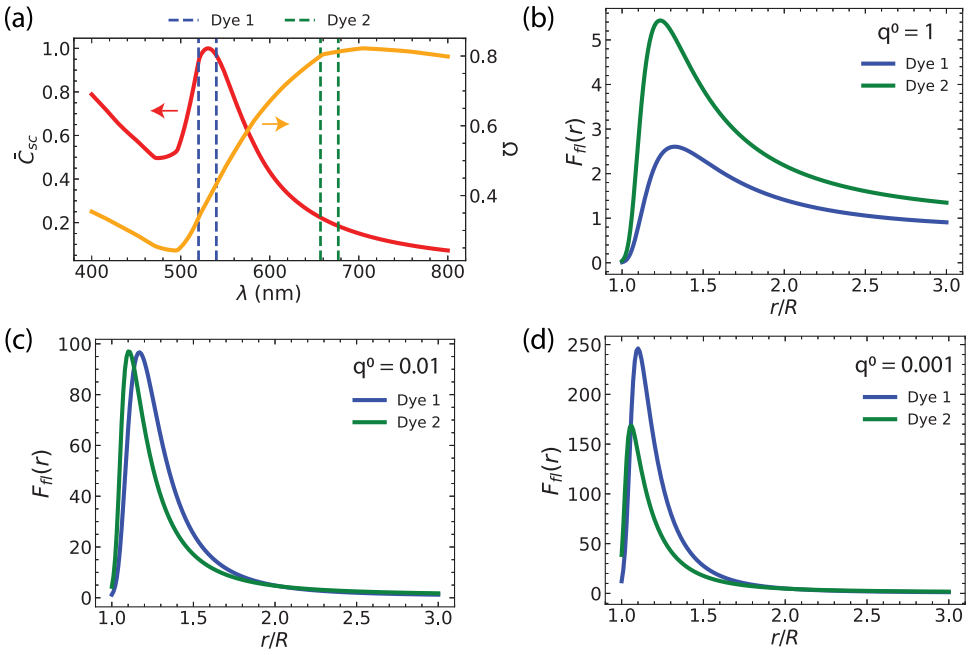


**Figure 5.** Optimal enhancement comparison between on- and off-resonance configurations with varying quantum yields. (a) Spectral configurations of two hypothetical dyes coupled to a gold spherical pNP with a radius of $R$ = 50 nm. Dye 1 exhibits an on-resonance configuration, with $\lambda_{abs}$ = 520 nm and $\lambda_{em}$ = 540 nm. In contrast, Dye 2 is in an off-resonance configuration, with $\lambda_{abs}$ = 657 nm and $\lambda_{em}$ = 677 nm. (b–d) Enhancement for both dyes is shown as a function of molecular position $r$ (in units of $R$), measured from the origin of the coordinate system, across three quantum yield values: $q^0$ = 1, 0.01, 0.001, respectively.

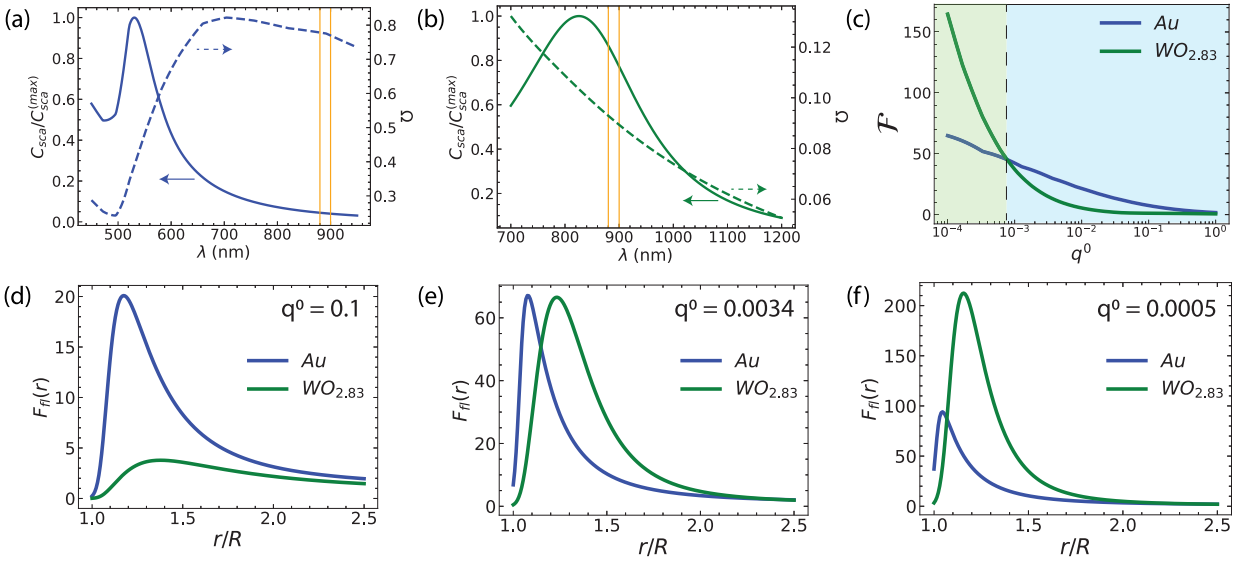


**Figure 6.** Optimal enhancement comparison between two plasmonic materials for a given spectral configuration of the molecule with a varying quantum yield. (a, b) Normalized scattering cross section $\bar{C}_{sc}$, and scattering-to-extinction ratio Ω, for Au and $WO_{2.83}$ pNPs, respectively. (c) Optimal enhancement factor, $\mathcal{F}$, as a function of quantum yield, showing the transition from a Au-maximally enhanced regime to a $WO_{2.83}$-maximally enhanced regime. (d–f) Distance dependence of the fluorescence enhancement factor $F_{fl}$, for three values of the quantum yield: $q^0$ = 0.1, 0.0034, 0.0005 respectively.

quantum yield, we pass a transition point when the magnitude of $F_{fl}$ for both dyes is identical (although the optimal distances differ). Finally, we enter in the $WO_{2.83}$-optimized zone for very small quantum yields. In Figure 6d–f, we have isolated $F_{fl}(r)$ for three quantum yields, $q^0$ = 0.1, 0.0034, 0.0005 respectively, thereby illustrating the described transition.

## CONCLUSIONS

This work provides new insights into enhancing the fluorescence rate of molecules. We have established an underlying link between the particle's optical response and the resulting optimal fluorescence enhancement. Specifically, we found that the molecular absorption and emission wavelengths for optimal enhancement correspond closely to the particle's scattering cross section and scattering-to-extinction ratio, respectively. This connection allows for a



https://doi.org/10.1021/acs.jpcc.4c08617
J. Phys. Chem. C 2025, 129, 4282–4289

deeper understanding of how the enhancement factor evolves with changes in the intrinsic quantum yield. For moderate quantum yields, it is essential to consider the particle's scattering efficiency relative to absorption, identifying spectral regions where this efficiency is maximized. This insight reveals that the optimal fluorescence enhancement can occur away from the plasmon resonance in this regime. Conversely, for low quantum yields, particle absorption is suppressed, and maximal enhancement is achieved near the plasmon resonance, i.e. a molecule at resonance with the pNP is the desired configuration. The provided examples complement these findings and offer valuable guidance for experimental applications, especially in the near- and mid-infrared ranges, where the energy-gap law plays a significant role.

## ■ ASSOCIATED CONTENT

### Data Availability Statement

The Jupyter notebook including the implementation of the analytical model and all the calculations is freely available on Zenodo at doi:10.5281/zenodo.14412018.

### Supporting Information

The Supporting Information is available free of charge at https://pubs.acs.org/doi/10.1021/acs.jpcc.4c08617.

Theoretical background, full analytical model, additional results on optimal enhancement spectral maps using the Drude model and other realistic materials, and impact of the quantum yield on the optimal enhancement for various particle sizes (PDF)

## ■ AUTHOR INFORMATION


### Corresponding Authors

**Stavros Athanasiou** − *Nanophotonics and Metrology Laboratory (NAM), Swiss Federal Institute of Technology Lausanne (EPFL), 1015 Lausanne, Switzerland;* orcid.org/0009-0002-8171-6838; Email: stavros.athanasiou@epfl.ch

**Olivier J. F. Martin** − *Nanophotonics and Metrology Laboratory (NAM), Swiss Federal Institute of Technology Lausanne (EPFL), 1015 Lausanne, Switzerland;* orcid.org/0000-0002-9574-3119; Email: olivier.martin@epfl.ch

Complete contact information is available at: https://pubs.acs.org/10.1021/acs.jpcc.4c08617


### Notes

The authors declare no competing financial interest.

## ■ ACKNOWLEDGMENTS

Funding from the Swiss National Science Foundation (project CRSII5_216629) is gratefully acknowledged. It is a pleasure to acknowledge insightful discussions with Elodie Didier, Joao Pedro Ferreira Assuncao, Roland Hany, Markus Niederberger, Frank Nüesch, Eleonora Radaelli, and Siarhei Zavatski.

## ■ REFERENCES


(1) Purcell, E. M. Spontaneous Emission Probabilities at Radio Frequencies. *Phys. Rev.* **1946**, *69*, 681.

(2) Benisty, H.; Greffet, J.; Lalanne, P. *Introduction to Nanophotonics*; Oxford University Press, Oxford graduate texts, 2022.

(3) Manjavacas, A.; García de Abajo, F. J.; Nordlander, P. Quantum plexcitonics: strongly interacting plasmons and excitons. *Nano Lett.* **2011**, *11*, 2318−2323.

(4) Stranius, K.; Hertzog, M.; Börjesson, K. Selective manipulation of electronically excited states through strong light−matter interactions. *Nat. Commun.* **2018**, *9*, 2273.

(5) Chance, R. R.; Prock, A.; Silbey, R. Lifetime of an excited molecule near a metal mirror: Energy transfer in the Eu3+/silver system. *J. Chem. Phys.* **1974**, *60*, 2184−2185.

(6) Kühn, S.; Håkanson, U.; Rogobete, L.; Sandoghdar, V. Enhancement of Single-Molecule Fluorescence Using a Gold Nanoparticle as an Optical Nanoantenna. *Phys. Rev. Lett.* **2006**, *97*, No. 017402.

(7) Anger, P.; Bharadwaj, P.; Novotny, L. Enhancement and Quenching of Single-Molecule Fluorescence. *Phys. Rev. Lett.* **2006**, *96*, No. 113002.

(8) Ayala-Orozco, C.; Liu, J. G.; Knight, M. W.; Wang, Y.; Day, J. K.; Nordlander, P.; Halas, N. J. Fluorescence enhancement of molecules inside a gold nanomatryoshka. *Nano Lett.* **2014**, *14*, 2926−2933.

(9) Krenn, J. R.; Dereux, A.; Weeber, J. C.; Bourillot, E.; Lacroute, Y.; Goudonnet, J. P.; Schider, G.; Gotschy, W.; Leitner, A.; Aussenegg, F. R.; et al. Squeezing the Optical Near-Field Zone by Plasmon Coupling of Metallic Nanoparticles. *Phys. Rev. Lett.* **1999**, *82*, 2590−2593.

(10) Oldenburg, S. J.; Averitt, R. D.; Westcott, S. L.; Halas, N. J. Nanoengineering of optical resonances. *Chem. Phys. Lett.* **1998**, *288*, 243−247.

(11) Tam, F.; Goodrich, G. P.; Johnson, B. R.; Halas, N. J. Plasmonic enhancement of molecular fluorescence. *Nano Lett.* **2007**, *7*, 496−501.

(12) Bharadwaj, P.; Novotny, L. Spectral dependence of single molecule fluorescence enhancement. *Opt. Express* **2007**, *15*, 14266−14274.

(13) Bardhan, R.; Grady, N. K.; Cole, J. R.; Joshi, A.; Halas, N. J. Fluorescence enhancement by Au nanostructures: nanoshells and nanorods. *ACS Nano* **2009**, *3*, 744−752.

(14) Kern, A. M.; Meixner, A. J.; Martin, O. J. F. Molecule-dependent plasmonic enhancement of fluorescence and Raman scattering near realistic nanostructures. *ACS Nano* **2012**, *6*, 9828−9836.

(15) Mayerhöffer, U.; Gsänger, M.; Stolte, M.; Fimmel, B.; Würthner, F. Synthesis and molecular properties of acceptor-substituted squaraine dyes. *Chemistry* **2013**, *19*, 218−232.

(16) Kamath, A.; Guyot-Sionnest, P. The "energy gap law" for mid-infrared nanocrystals. *J. Chem. Phys.* **2024**, *160*, 20.

(17) Englman, R.; Jortner, J. The energy gap law for radiationless transitions in large molecules. *Mol. Phys.* **1970**, *18*, 145−164.

(18) Jang, S. J. A simple generalization of the energy gap law for nonradiative processes. *J. Chem. Phys.* **2021**, *155*, 164106.

(19) Sajjad, M. T.; Manousiadis, P. P.; Chun, H.; Vithanage, D. A.; Rajbhandari, S.; Kanibolotsky, A. L.; Faulkner, G.; O'Brien, D.; Skabara, P. J.; Samuel, I. D. W.; et al. Novel fast color-converter for visible light communication using a blend of conjugated polymers. *ACS Photonics* **2015**, *2*, 194−199.

(20) Zampetti, A.; Minotto, A.; Cacialli, F. Near-infrared (NIR) organic light-emitting diodes (OLEDs): Challenges and opportunities. *Adv. Funct. Mater.* **2019**, *29*, 1807623.

(21) Cosco, E. D.; Caram, J. R.; Bruns, O. T.; Franke, D.; Day, R. A.; Farr, E. P.; Bawendi, M. G.; Sletten, E. M. Flavylium polymethine fluorophores for near- and shortwave infrared imaging. *Angew. Chem., Int. Ed. Engl.* **2017**, *56*, 13126−13129.

(22) Zhu, S.; Tian, R.; Antaris, A. L.; Chen, X.; Dai, H. Near-infrared-II molecular dyes for cancer imaging and surgery. *Adv. Mater.* **2019**, *31*, No. e1900321.

(23) Vahedigharehchopogh, N.; Kıbrıslı, O.; Erol, E.; Çelikbilek Ersundu, M.; Ersundu, A. E. A straightforward approach for high-end anti-counterfeiting applications based on NIR laser-driven lanthanide doped luminescent glasses. *J. Mater. Chem. C Mater. Opt. Electron. Devices* **2021**, *9*, 2037−2046.

(24) Athanasiou, S.; Martin, O. J. F. Analytical Model for Modification of Fluorescence of Quantum Emitters near a Spherical Particle [Computational Notebooks]. *Zenodo* **2024**,.

(25) Mie, G. Beiträge zur Optik trüber Medien, speziell kolloidaler Metallösungen. *Ann. Phys.* **1908**, *330*, 377−445.
(26) Bohren, C.; Huffman, D. *Absorption and Scattering of Light by Small Particles*; Wiley Science Series; Wiley, 2008.
(27) Chew, H.; McNulty, P. J.; Kerker, M. Model for Raman and fluorescent scattering by molecules embedded in small particles. *Phys. Rev. A* **1976**, *13*, 396−404.
(28) Chew, H. Transition rates of atoms near spherical surfaces. *J. Chem. Phys.* **1987**, *87*, 1355−1360.
(29) Arruda, T. J.; Bachelard, R.; Weiner, J.; Slama, S.; Courteille, P. W. Fano resonances and fluorescence enhancement of a dipole emitter near a plasmonic nanoshell. *Phys. Rev. A* **2017**, *96*, No. 043869.
(30) Johnson, P. B.; Christy, R. W. Optical Constants of the Noble Metals. *Phys. Rev. B* **1972**, *6*, 4370−4379.
(31) Walhorn, V.; Paskarbeit, J.; Frey, H. G.; Harder, A.; Anselmetti, D. Distance dependence of near-field fluorescence enhancement and quenching of single quantum dots. *Beilstein J. Nanotechnol.* **2011**, *2*, 645−652.
(32) Zuloaga, J.; Nordlander, P. On the energy shift between near-field and far-field peak intensities in localized plasmon systems. *Nano Lett.* **2011**, *11*, 1280−1283.
(33) Esteban, R.; Borisov, A. G.; Nordlander, P.; Aizpurua, J. Bridging quantum and classical plasmonics with a quantum-corrected model. *Nat. Commun.* **2012**, *3*, 825.
(34) Ciracì, C.; Jurga, R.; Khalid, M.; Della Sala, F. Plasmonic quantum effects on single-emitter strong coupling. *Nanophotonics* **2019**, *8*, 1821−1833.
(35) Gonçalves, P. A. D.; Christensen, T.; Rivera, N.; Jauho, A.-P.; Mortensen, N. A.; Soljačić, M. Plasmon-emitter interactions at the nanoscale. *Nat. Commun.* **2020**, *11*, 366.
(36) Manthiram, K.; Alivisatos, A. P. Tunable localized surface plasmon resonances in tungsten oxide nanocrystals. *J. Am. Chem. Soc.* **2012**, *134*, 3995−3998.



https://doi.org/10.1021/acs.jpcc.4c08617
J. Phys. Chem. C 2025, 129, 4282−4289